Copy
RM L57E09

NACA RM L57E09

NACA

RESEARCH MEMORANDUM

TRANSONIC FLUTTER CHARACTERISTICS OF A CAMBERED
A-PLAN-FORM WING WITH AND WITHOUT
SIMULATED NACELLES

By H. Neale Kelly

Langley Aeronautical Laboratory
Langley Field, Va.

NATIONAL ADVISORY COMMITTEE
FOR AERONAUTICS

WASHINGTON
July 10, 1957

NATIONAL ADVISORY COMMITTEE FOR AERONAUTICS

RESEARCH MEMORANDUM

TRANSONIC FLUTTER CHARACTERISTICS OF A CAMBERED A-PLAN-FORM WING WITH AND WITHOUT SIMULATED NACELLES

By H. Neale Kelly

SUMMARY

An experimental investigation has been made in the Langley transonic blowdown tunnel to determine the effects of simulated engine nacelles on the flutter characteristics of a cambered A-plan-form wing with 45° sweepback of the leading edge, an aspect ratio of 3.6, and a taper ratio of 0.14. The simulated engine nacelles were attached at the 0.60- and 0.80-semispan stations immediately adjacent to the lower surface of the wing.

Data obtained with the wing rigidly mounted in the tunnel indicated that the addition of the nacelles produced significant increases in the flutter speed of the wing. Attempts to determine the flutter characteristics of the model in a mount which allowed freedom in roll and vertical translation produced only meager and inconclusive results because of inherent difficulties associated with testing a cambered wing with these degrees of freedom of the mount.

INTRODUCTION

Low-speed flutter investigations have indicated that the addition of concentrated weights, such as engine nacelles, and the introduction of body freedoms (especially if the wing mass and inertia are large relative to the fuselage mass and inertia) can produce marked changes in the flutter characteristics of a wing. (See, for example, refs. 1, 2, and 3.) Little information is available, however, on the effects of these variables on the flutter characteristics of wings at transonic speeds.

Accordingly, an investigation has been made in the Langley transonic blowdown tunnel to determine the effects of the addition of simulated nacelles on the flutter characteristics of a model of a proposed bomber wing. An attempt was also made to determine the effects of body freedom in roll and vertical translation through the use of a special wing-mounting system. The results of the investigation and a limited analysis are presented herein.

SYMBOLS

b	wing semichord
f	frequency of oscillation, cps
f_i	measured coupled natural frequencies, cps; $i = 1, 2, 3, \ldots 8$
I	mass moment of inertia, slug-ft^2
m	mass, slugs
M	free-stream Mach number
q	free-stream dynamic pressure, lb/sq in.
T	free-stream temperature, $^{\circ}$Rankine
V	free-stream velocity, ft/sec
ρ	free-stream density, slugs/cu ft
ω	frequency of oscillation, radians/sec
ω_α	fundamental torsional frequency, radians/sec
ω_n	natural frequency, radians/sec
K	linear spring constant, lb/ft
τ	rotational spring constant, ft-lb/radian

MODELS

Eight wings of identical plan form and construction were expended in the course of the present investigation. Five of the wings were equipped with simulated engine nacelles; the other three were tested without nacelles.

Configuration

The basic A-plan-form wing (see fig. 1) had an aspect ratio of 3.59, a taper ratio of 0.14, and a 45° sweptback leading edge. It was formed by the addition of a straight-trailing-edge chord-extension to the inboard portion of a sweptback wing that had an aspect ratio of 3.70 and a taper ratio of 0.15. The modified NACA 65-series cambered airfoil sections of the swept wing (see table I) were further modified to form the A-plan-form airfoil sections by fairing a tangent to the upper surface of the wing from the trailing edge of the trailing-edge chord-extension. Streamwise thickness ratios of the resulting airfoil sections varied from 0.04 at the root to 0.03 at the tip.

The simulated nacelles (fig. 1) were rigidly attached immediately adjacent to the lower surface of the wing at the 0.60- and 0.80-semispan stations. No flow was simulated through the simplified nacelles, which consisted of a cylindrical midsection with conical ends.

Scaling

The models were 0.022-size, dynamically and elastically scaled versions of a proposed airplane wing. For convenience the mass and stiffness of the models were scaled so that at any given Mach number the dynamic pressure at a given simulated altitude was twice as great as the dynamic pressure for that altitude in the NACA standard atmosphere. (See ref. 4.) This scaling was accomplished by duplicating the airplane reduced velocity (based on ω_α) $V/b\omega_\alpha$ and the mass ratio $m/\pi\rho b^2$, with the assumption that at every simulated altitude the tunnel temperature was the same as that for the standard atmosphere. This assumption is not quite correct since the tunnel temperature is a function of the amount of air expended from the reservoir during the course of a run. Because of this difference in temperature, the reduced velocity and mass ratio are not individually duplicated. However, the difference in temperature does not affect the simulation of the dynamic pressure, which is proportional to the product of the square of the reduced velocity and the inverse of the mass ratio.

Construction

The main load-carrying structure of the wing (figs. 1 and 2) consisted of a single formed-aluminum box spar, stabilized with foam plastic, to which a perforated web was attached. Aluminum ribs and magnolia-wood leading and trailing edges completed the structural framework. The entire structure was bonded with an epoxy resin. Low-strength balsa (with grain oriented as indicated in fig. 1) bonded to the framework was used to obtain the desired contour, and the entire wing was covered with Japanese tissue and aircraft dope.

The simulated nacelles were turned from magnesium rods and were ballasted with lead weights as indicated in figure 1. Two screws and an epoxy resin bond were used to attach each nacelle to the wing.

Mount

As illustrated by the exploded drawing of figure 3, the wing mount consisted of a parallelogram linkage which provided freedom in vertical translation but restraint in pitch for a cradle which permitted freedom in roll. Soft coil springs located above and below the mount were provided for centering in the translational degree of freedom; in roll the centering spring consisted of a single cantilever beam. The amount of restraint in both degrees of freedom could be varied through the use of interchangeable springs. Adjustable stops provided a means of limiting or eliminating the travel in either or both of the degrees of freedom. Contact with these stops during the flutter tests was indicated through a set of fouling switches which (1) operated a fouling light visible to the test engineer and (2) simultaneously displaced a trace on the oscillograph record of the run. Angle-of-attack and angle-of-roll adjustment screws provided a means of setting the static angle of attack and angle of roll of the wing with respect to the fuselage.

Physical Properties

Natural frequencies and node lines.- Measured natural frequencies and typical node lines of the wings are presented in table II(a) for the wings with nacelles and table II(b) for the wings without nacelles. These data were obtained by exciting the wing with an electromagnetic shaker and observing the action of salt crystals sprinkled over the wing surface and the response of electrical wire strain gages affixed to the spar near the wing root.

Data in table II labeled "Wings rigidly clamped" were obtained with the wing spar root rigidly clamped to a massive table through the use of a clamping fixture similar to the wing spar holder and cap shown in figure 3. The method of clamping cantilevered the wing spar; however, the unclamped carryover structure at the leading and trailing edges permitted the excitation of antisymmetrical modes. In order to exclude the antisymmetrical modes the wings were forced to vibrate in the symmetrical modes through the use of a two-prong shaker stem which excited both panels of the wing at the point of intersection of the innermost rib and the trailing-edge chord-extension. (See table II.) Frequencies and node lines for wing 3, which are not presented, were similar to those listed for the other wings.

Representative wings (wing 4 with nacelles and wing 6 without) were placed in the wing mount and vibrated with and without various degrees of freedom of the mount. For these tests a single-prong shaker stem was used to excite the wing at the point of intersection of the innermost rib and the trailing-edge chord-extension of one of the wing panels. Symmetry or antisymmetry was determined by placing the strain-gage signals from the two wing panels on an oscilloscope screen in such a manner that symmetric modes produced a figure with its axis in the first and third quadrants; antisymmetric modes, in the second and fourth quadrants. In addition, at the low frequencies, the model motions were observed through the use of a stroboscopic light.

Mass and inertia.- Experimentally determined mass and inertia properties of streamwise strips of a representative wing are presented in table III. The data do not include the material removed in cutting the wing into strips. Table IV contains the mass and inertia properties of the basic nacelles. Attachment screws not included in the basic nacelle data shifted the center of gravity rearward 0.03 to 0.04 inch. Ratios of the mass and moment of inertia of both nacelles to the exposed-wing mass and moment of inertia (both moments of inertia referred to the local wing-spar axis) are 0.56 and 0.52, respectively.

The effective mass and moment of inertia of the spring-supported wing mount depends upon the frequency of the flutter mode and can be determined from the following general relations:

$$m = K \frac{\omega^2 - \omega_n^2}{\omega^2 \omega_n^2} \qquad\qquad I = \tau \frac{\omega^2 - \omega_n^2}{\omega^2 \omega_n^2}$$

where K and τ are spring constants, ω is the frequency of oscillation, and ω_n is the appropriate natural frequency of the system. Experimentally determined spring constants and appropriate natural frequencies of the mount (vertical translation and roll, respectively) have been used in the above equations to determine the effective mass and rolling moment of inertia of the wing mount for the range of flutter frequencies. The results are presented in graphical form in figure 4.

Influence coefficients.- Structural influence coefficients measured at 24 points (located as indicated in fig. 5 on wing 7) are presented in matrix form in table V(a). The experimental techniques utilized in obtaining these data are the same as those employed in reference 5 and are fully described therein. A symmetrical matrix of influence coefficients (table V(b)) has been formed by averaging corresponding off-diagonal elements of the measured matrix (table V(a)). In table V(a), 85 percent of the off-diagonal elements are within 2 percent of the average (table V(b)) and 97 percent are within 5 percent of the average.

The symmetrical matrix, together with the associated masses of the various segments listed in figure 5, has been used in the calculation of the first three natural frequencies and corresponding symmetrical mode shapes of the cantilevered wing. (Masses listed in fig. 5 are experimentally determined values adjusted to compensate for material removed in cutting the wing into segments.) Calculated natural frequencies and mode shapes determined by the method outlined in reference 6 are presented in table VI. Node lines of the calculated modes (not presented) are in substantial agreement with those of table II(b). A comparison of the calculated and measured frequencies can be obtained from the following table:

Mode	Measured frequency, cps	Calculated frequency, cps	Percent deviation
f_2	110	113.2	2.9
f_4	370	347	-6.2
f_6	483	535	10.7

FACILITIES AND TESTS

Experimental results presented herein were obtained in the Langley transonic blowdown tunnel. The tunnel, which has a 26-inch, octagonal, slotted test section can be operated throughout the transonic speed range at air densities from approximately 0.001 to 0.012 slug per cubic foot.

Support for the wings was furnished by the wing mount, which was housed in a $1\frac{1}{4}$- by $4\frac{1}{4}$-inch sting (see figs. 3 and 6). The nose of this sting extended forward of the model, along the tunnel center line, into the subsonic region of the tunnel without change in cross section to prevent the formation of a bow shock which might be reflected onto the model by the tunnel walls. The fundamental frequency of the sting is estimated to be approximately 15 cps.

The test procedure for all runs was the same: The Mach number control valve downstream of the test section was set to obtain the desired Mach number; then, upstream valves between the tunnel and a high-pressure reservoir were slowly opened and the tunnel stagnation pressure was increased until flutter or divergence occurred. (A system of interchangeable orifice plates formerly used to control the Mach number has been supplanted by a motorized gate-type valve.) Tests with body freedoms were made with the model set at the angle of attack required to center the wing and mount between the upper and lower translation stops, as determined by low-pressure trim runs. For the tests with body freedoms locked out the wings were set at an angle of attack of approximately 1.5°, except for run 17, where the angle was approximately 0°. A multichannel oscillograph provided a continuous record of the test conditions and the behavior of resistance-type strain gages attached to the wing surface. Two high-speed (approximately 1,000 frames per second) 16-mm motion-picture cameras running in sequence furnished a record of the model motions.

RESULTS AND DISCUSSION

The results of tests of the models with the wing mount fixed and free are presented in tables VII and VIII, respectively. Data from tests of a wall-mounted semispan wing of identical dimensions and construction conducted in the Langley 9- by 18-inch supersonic flutter tunnel at a Mach number of 1.3 are also presented in table VII. The tables are chronological records of the more important events occurring during each run. Code letters, defined at the head of each table, are used to describe the behavior of the model.

Sudden divergence and failure of models was usually encountered in the tests with the mount either fixed or free whenever the model attitude was such that an untrimmed pitching moment existed on the wing. Failure of this type was responsible for the complete destruction of the models which terminated run 17 (table VII) and runs 10 and 11 (table VIII) and resulted in damage during run 12 (table VIII). Observation of these runs and the remains of the models indicated that the failure stemmed from the untrimmed negative pitching moment about the spar, which caused the leading edge of the wing to twist downward, resulting in a large negative effective angle of attack that overloaded the wing and caused it to bend downward and fail.

Model With Wing-Mount Fixed

The initial run with the wing-mount fixed (run 17) was made at zero angle of attack. As noted in the preceding paragraph, this run was terminated abruptly by the sudden divergence and destruction of the model. (Oscillograph records indicate no oscillatory motion immediately prior to destruction.) For subsequent tests with the wing-mount fixed, the angle of attack was, therefore, increased to approximately 1.5° to reduce the magnitude of the negative pitching moment.

In run 17 it is interesting to note that although the left wing, which was visible to the test engineer during the run, collapsed as the wing bent downward, motion pictures of the right wing show clearly that the right wing was destroyed when it was struck by the left wing. Selected frames from the high-speed motion pictures, presented in figure 7, admittedly do not offer as graphic evidence as does the motion picture. However, they show the right wing being destroyed by the left wing, which wraps underneath the sting fuselage (note the left wing underneath the sting at 0.0038 second) and strikes the right wing near the inboard nacelle.

Flutter was encountered during all subsequent runs with the mount fixed. As indicated by the oscillograph record of a typical run shown in figure 8, the amplitude of the oscillation built up rapidly, and the model was usually destroyed before shutdown of the tunnel could be accomplished. As illustrated by the sequence of pictures for runs 18, 19, and 23 shown in figure 7, breakup of the models at an angle of attack of 1.5° was, however, much more gradual than the sudden divergence and explosive disintegration encountered at an angle of attack of 0° (run 17). Initial failure of the wings with nacelles, as shown by the figure, always occurred at a point just inboard of the nacelles. It can be seen from figure 1 that the point of failure coincides with the end of the trailing-edge chord extension and the rearward bend in the spar.

Data from table VII have been used to prepare figure 9. In this figure significant results of the tests are presented on a plot of dynamic pressure against Mach number, across which lines of constant simulated altitude (see section entitled "Scaling") have been drawn. Comparison of the nacelle-off and nacelle-on data indicates that the addition of nacelles increased the dynamic pressure required for flutter. At a Mach number of approximately 0.65 the nacelles increased the critical dynamic pressure by approximately 70 percent; at a Mach number of 1.3 the semispan-wing data obtained in the 9- by 18-inch supersonic flutter tunnel indicate that the nacelles caused an increase of over 80 percent.

Model With Wing Mount Free

Results of the tests with the wing mount free to roll and to translate vertically are somewhat meager and inconclusive because of inherent difficulties encountered during the tests. These difficulties apparently sprang from the use of a cambered wing section, which made it impossible to trim the wing lift and pitching moment simultaneously. When not at zero lift the mount banged against the stops, introducing extraneous vibratory stresses and strains which obscured the wing strain-gage records. At zero lift the attendant negative pitching moment precipitated the sudden divergence and failure mentioned previously. Satisfactory operation of the mount during flutter tests of an uncambered wing of similar plan form further indicated that the difficulties stemmed primarily from the use of a cambered wing.

Because of these difficulties, a flutter boundary for the wing with nacelles was not established. However, points designating the start of irregular high-frequency (700 to 1,000 cps) oscillation, believed to be associated with the models hitting the stops, and bursts of low-amplitude regular sinusoidal oscillations are indicated in table VIII and figure 10. Three points of probable flutter - a start of flutter for runs 11 and 13 and an end of flutter for run 11 (see table VIII and fig. 10) - describe a tentative flutter boundary for the wings without nacelles. These flutter points, together with all other regular sinusoidal oscillations encountered in the course of the investigation, occurred in a symmetric mode.

CONCLUDING REMARKS

The results of transonic flutter tests of the cambered A-plan-form wing with and without simulated engine nacelles indicated that the addition of nacelles increased the dynamic pressure required for flutter. This increase appeared to be larger at the higher Mach numbers.

The results of tests in a mount which allowed freedom in roll and in vertical translation were meager and inconclusive because of inherent difficulties associated with flutter-testing a cambered wing with these degrees of freedom of the mount.

Langley Aeronautical Laboratory,
National Advisory Committee for Aeronautics,
Langley Field, Va., April 12, 1957.

REFERENCES

1. Martina, Albert P., and Young, George E.: Results of Initial Wind-Tunnel Flutter Experiments at Low Speed With a Towed Airplane Model Having a 40° Sweptback Wing of Aspect Ratio 3.62 Equipped With Pylon-Mounted Stores. NACA RM L54K17, 1955.

2. Gaukroger, D. R.: Wind-Tunnel Tests on the Symmetric and Antisymmetric Flutter of Swept-Back Wings. R. & M. No. 2911, British A.R.C, Mar. 1955.

3. Runyan, Harry L., and Watkins, Charles E.: Flutter of a Uniform Wing With an Arbitrarily Placed Mass According to a Differential-Equation Analysis and a Comparison With Experiment. NACA Rep. 966, 1950. (Supersedes NACA TN 1848.)

4. The Staff of the Ames 1- by 3-Foot Supersonic Wind-Tunnel Section: Notes and Tables for Use in the Analysis of Supersonic Flow. NACA TN 1428, 1947.

5. Jones, George W., Jr., and Young, Lou S., Jr.: Transonic Flutter Investigation of Two 64° Delta Wings With Simulated Streamwise Rib and Orthogonal Spar Construction. NACA RM L56I27, 1957.

6. Scanlan, Robert H., and Rosenbaum, Robert: Introduction to the Study of Aircraft Vibration and Flutter. The MacMillan Co., 1951.

TABLE I.- STREAMWISE AIRFOIL ORDINATES

[Dimensions in inches]

Root*			Tip		
Station	Ordinate		Station	Ordinate	
	Upper	Lower		Upper	Lower
0	0.005	0	0	0	0
.189	.079	.026	.028	.008	.003
.377	.118	.030	.057	.012	.003
.755	.167	.039	.113	.017	.004
1.132	.197	.048	.170	.020	.005
1.509	.216	.056	.226	.022	.006
2.264	.238	.073	.340	.025	.008
3.019	.244	.084	.453	.025	.009
3.774	.234	.083	.566	.024	.009
4.528	.206	.070	.679	.021	.007
5.283	.163	.053	.792	.017	.005
6.038	.111	.035	.906	.012	.004
6.792	.056	.018	1.019	.006	.002
7.547	.003	.002	1.132	.003	.002
Leading-edge radius: 0.013			Leading-edge radius: 0.0014		

*Wing without trailing-edge chord-extension.

TABLE II.- NATURAL FREQUENCIES AND NODAL LINES

(a) Wings with nacelles.

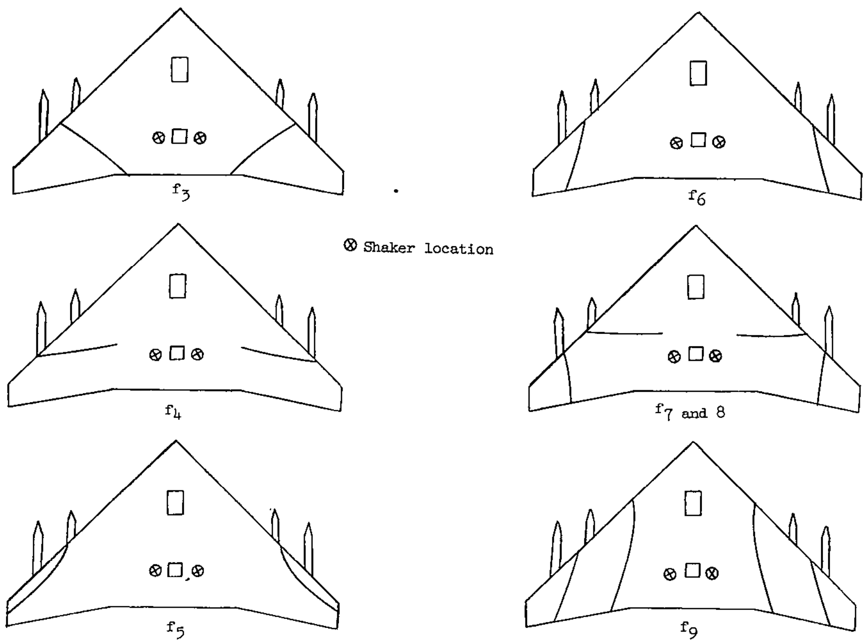

Typical nodal lines

Mode		Wings rigidly clamped				Wing number 4 in mount			
		Wing number				Mount freedom			
		1	2	3	4	None	Roll	Vertical translation	Roll and translation
						Mount frequency (wing installed)			
Roll							16		17
Translation								27	28
Yaw						158	162	209	
						Wing elastic frequency			
f_1	Antisymmetrical					47		48	
f_2	Symmetrical	77	77	---	78	79	79	83	83
f_3	Antisymmetrical						167	172	165
f_4	Symmetrical	180	181	---	177	177	182	178	182
f_5	Antisymmetrical					242	222		222
f_6	Symmetrical	312	322	---	317	316	316	334	338
f_7	Antisymmetrical						409(weak)	402	402
f_8	Symmetrical	412	433	---	407	410			409
f_9	Antisymmetrical					567	520(weak)	513	509

TABLE II.- NATURAL FREQUENCIES AND NODAL LINES - Concluded

(b) Wings without nacelles.

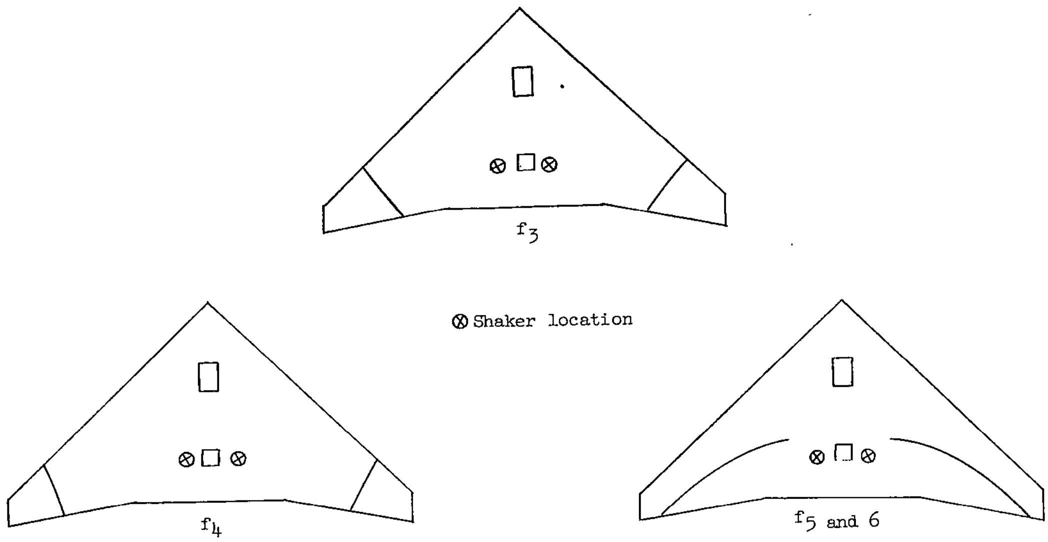

Typical nodal lines

Mode		Wings rigidly clamped				Wing number 6 in mount			
		Wing number				Mount freedom			
		5	6	7	8	None	Roll	Vertical translation	Roll and translation
						Mount frequency (wing installed)			
	Roll						26		27
	Translation							32	31
	Yaw					191			
						Wing elastic frequency			
f_1	Antisymmetrical					84	79(weak)	70	60
f_2	Symmetrical	109	111	110	106	110	110	114	114
f_3	Antisymmetrical					273	213	239	228
f_4	Symmetrical	360	373	370	352	368	362	383	386
f_5	Antisymmetrical					471	465	462	463
f_6	Symmetrical	490	500	483	454	483	478	478(weak)	475(weak)

TABLE III.- MASS AND INERTIA PROPERTIES OF REPRESENTATIVE WING

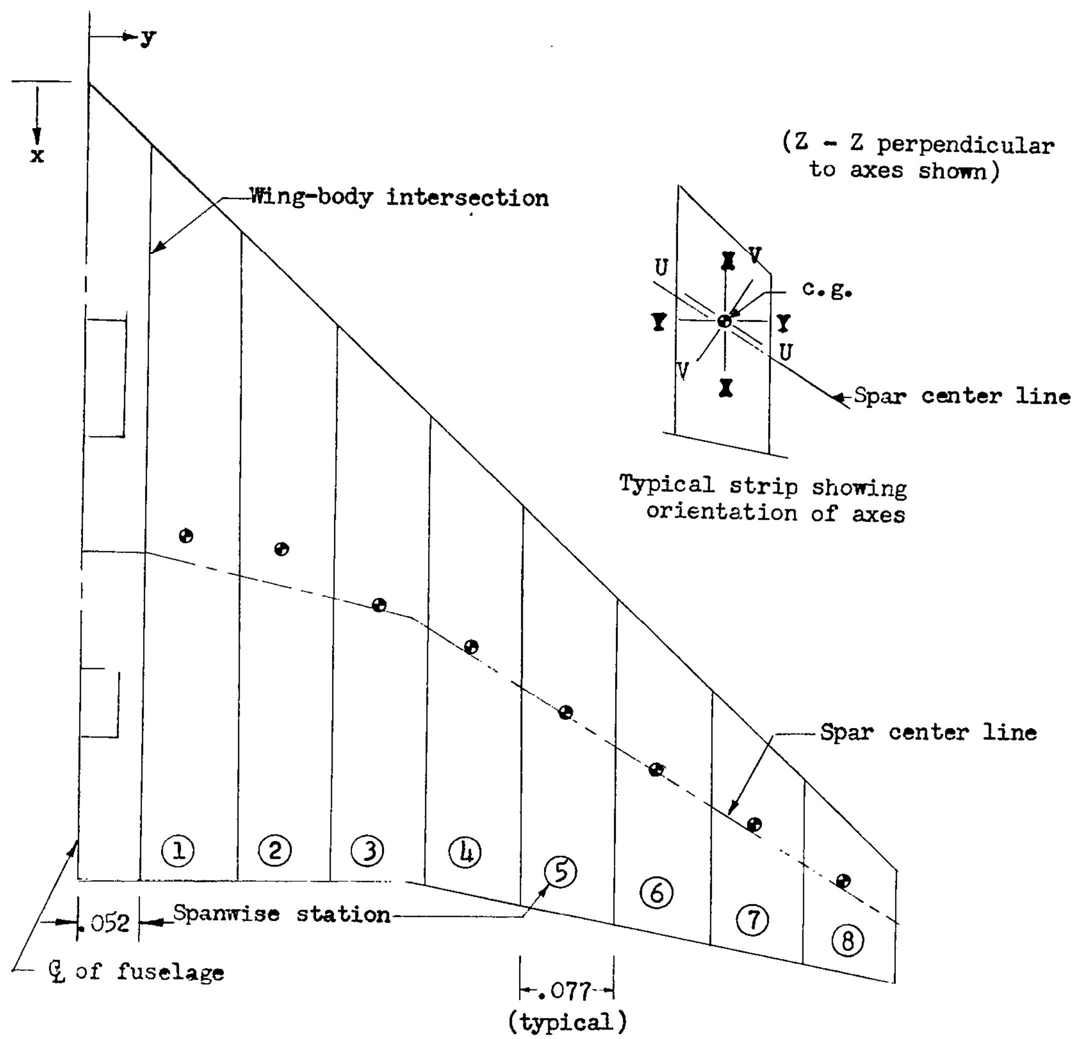

Spanwise station	Mass, slugs	c.g. location, in.		$I_{cg} \times 10^6$, slug-ft^2				
		x	y	Y - Y	X - X	Z - Z	U - U	V - V
1	0.000584	4.65	1.06	12.65	0.32	12.99	12.17	1.10
2	.000448	4.80	1.95	7.36	.24	7.40	6.39	.63
3	.000357	5.36	2.92	3.69	.19	3.71	3.15	.45
4	.000298	5.76	3.83	2.29	.15	2.33	1.73	.95
5	.000255	6.42	4.77	1.19	.13	1.25	.78	.60
6	.000190	6.98	5.66	.65	.11	.71	.41	.30
7	.000149	7.55	6.62	.26	.06	.32	.17	.17
8	.000081	8.13	7.49	.08	.04	.12	.05	.06

[redacted]

TABLE IV.- MASS AND INERTIA PROPERTIES OF NACELLES

Wing number	Left wing				Right wing			
	Outboard		Inboard		Inboard		Outboard	
	Mass, slugs	*$I_{cg} \times 10^6$, slug-ft^2	Mass, slugs	*$I_{cg} \times 10^6$, slug-ft^2	Mass, slugs	*$I_{cg} \times 10^6$, slug-ft^2	Mass, slugs	*$I_{cg} \times 10^6$, slug-ft^2
1	0.000671	4.32	0.000681	4.75	0.000681	4.71	0.000671	4.53
2	.000659	4.53	.000681	4.75	.000684	4.96	.000668	4.53
3	.000684	4.75	.000687	4.75	.000681	4.96	.000668	4.32
4	.000681	4.53	.000684	4.75	.000668	4.75	.000668	4.53
8	Not measured							

*Moment of inertia about the lateral axis through the nacelle center of gravity.

[redacted]

[redacted]

TABLE V.- MEASURED AND AVERAGED INFLUENCE COEFFICIENTS

(a) Measured influence coefficients, $\frac{ft}{lb} \times 10^5$, at load point -

Deflection Point	11	12	13	21	22	23	31	32	33	41	42	43	51	52	53	61	62	63	71	72	73	81	82	83
11	15.8	1.26	-1.04	7.99	1.83	-1.31	3.84	1.64	-0.515	2.82	1.16	-0.570	1.91	0.705	-0.774	1.53	-0.468	-1.16	0	0	-1.37	-0.369	-1.22	-2.06
12	1.22	9.63	1.37	2.39	2.73	1.68	3.39	3.43	3.19	4.76	4.53	3.91	5.80	5.36	4.84	7.43	6.12	6.33	7.40	7.63	7.20	8.97	7.83	7.61
13	-1.03	1.37	21.7	-.542	2.45	12.6	.580	3.64	9.48	3.95	4.94	7.17	4.82	7.61	9.28	7.33	7.76	9.81	9.19	10.8	12.6	10.9	11.6	12.8
21	8.10	2.31	-.527	15.9	4.71	.414	12.2	7.03	3.16	13.1	7.46	4.52	10.9	8.08	5.63	11.6	8.41	6.64	11.7	10.7	10.8	12.2	10.6	11.1
22	1.92	2.65	2.34	4.65	16.5	6.16	8.78	9.66	9.45	14.2	11.4	12.7	15.5	19.1	19.8	20.1	20.4	23.6	20.3	26.9	27.5	25.0	25.3	25.4
23	-1.28	1.81	13.0	.352	6.18	36.6	3.26	11.0	24.3	8.98	14.6	25.0	16.1	22.3	28.6	23.9	28.9	33.2	30.3	35.1	39.5	37.9	41.2	44.5
31	3.78	3.24	.589	12.2	8.84	3.50	25.1	15.8	9.17	26.6	20.1	14.4	29.5	24.5	19.9	28.4	25.9	22.7	35.3	32.4	30.0	37.9	38.0	33.5
32	1.70	3.45	3.91	7.05	10.2	11.2	15.4	25.8	20.2	24.4	25.7	27.9	33.5	34.9	37.8	42.3	43.3	47.5	49.0	50.6	56.1	55.6	59.9	60.2
33	-.663	3.10	9.46	2.72	9.43	24.3	9.17	19.6	54.5	19.3	31.3	47.9	33.9	45.2	59.5	51.4	59.6	70.4	65.3	71.6	83.4	81.0	85.5	92.0
41	2.79	5.15	3.98	13.0	14.0	8.93	26.5	24.3	19.4	50.6	35.2	29.7	50.9	47.3	43.4	57.3	52.2	49.4	67.6	63.0	66.1	74.2	78.8	67.1
42	1.16	4.51	4.94	6.99	11.3	14.5	19.9	25.1	31.5	34.7	54.6	47.8	54.8	62.1	67.1	77.6	80.4	82.5	94.4	98.3	103	114	115	116
43	-.663	3.70	6.67	4.56	12.5	24.4	14.4	28.2	48.9	29.5	46.7	92.9	55.1	77.6	105	84.7	104	125	112	128	146	142	155	163
51	1.88	5.86	4.67	10.9	15.5	17.1	28.9	33.3	32.8	51.3	53.4	55.1	96.0	80.7	78.6	106	107	109	132	134	135	155	154	155
52	.651	5.35	8.10	8.15	18.7	23.4	25.2	33.7	45.1	46.9	63.6	80.6	83.3	109	116	127	141	151	160	175	188	206	220	221
53	-.711	4.87	9.18	5.57	19.5	29.4	19.9	37.8	61.1	42.4	66.8	106	82.1	116	176	131	170	215	192	212	259	248	272	319
61	1.38	7.40	8.03	11.7	20.3	25.3	29.4	43.2	51.3	56.6	78.6	84.4	107	131	128	176	179	182	231	226	244	272	278	284
62	-.332	5.76	7.72	8.43	20.7	29.6	25.9	42.0	61.7	53.9	79.1	106	106	137	166	176	221	240	263	276	331	340	373	398
63	-1.20	6.20	9.04	6.59	23.6	34.1	23.0	46.5	69.0	48.0	81.7	124	108	146	206	182	233	328	291	345	412	378	448	510
71	0	7.57	8.06	11.7	20.9	30.2	35.9	47.4	65.1	67.5	94.3	114	136	157	190	230	262	292	355	391	411	492	511	536
72	0	8.55	11.3	10.7	25.4	36.5	32.4	51.0	74.6	64.8	95.2	128	132	168	206	231	282	343	388	439	492	556	591	643
73	-1.33	7.82	12.6	10.9	27.7	39.7	30.5	56.7	83.8	68.1	102	153	139	181	258	245	326	426	420	492	659	606	666	757
81	-.343	8.84	10.9	11.7	24.9	38.0	36.4	55.4	79.5	74.9	114	140	156	198	239	278	329	377	478	529	591	722	763	811
82	-1.38	7.46	12.0	10.1	25.2	40.6	38.1	62.3	85.1	77.6	118	154	156	218	263	280	365	432	495	564	665	745	825	924
83	-2.00	7.61	12.8	11.3	25.4	44.4	33.6	58.8	91.8	69.6	115	167	155	216	321	288	413	503	514	616	752	812	936	1150

(b) Averaged influence coefficients, $\frac{ft}{lb} \times 10^5$, at load point -

Deflection Point	11	12	13	21	22	23	31	32	33	41	42	43	51	52	53	61	62	63	71	72	73	81	82	83
11	15.8	1.24	-1.04	8.04	1.88	-1.30	3.81	1.67	-0.589	2.80	1.16	-0.616	1.90	0.678	-0.742	1.46	-0.400	-0.118	0	0	-1.35	-0.356	-1.30	-2.03
12		9.63	1.37	2.35	2.69	1.74	3.32	3.44	3.14	4.95	4.52	3.80	5.83	5.36	4.86	7.42	5.94	6.26	7.48	8.09	7.51	8.90	7.64	7.61
13			21.7	-.534	2.40	12.8	.584	3.78	9.47	3.96	4.94	6.92	4.74	7.86	9.23	7.68	7.74	9.42	8.62	11.0	12.6	10.9	11.8	12.8
21				15.9	4.68	.383	12.2	7.04	2.94	13.0	7.22	4.54	10.9	8.12	5.60	11.6	8.42	6.62	11.7	10.7	10.8	12.0	10.4	11.2
22					16.5	6.17	8.81	9.93	9.44	14.1	11.4	12.6	15.5	18.9	19.6	20.2	20.6	23.6	20.6	26.2	27.6	25.0	25.2	25.4
23						36.6	3.38	11.1	24.3	8.96	14.6	24.7	16.6	22.8	29.0	24.6	29.2	33.6	30.2	35.8	39.6	38.0	40.9	44.4
31							25.1	15.6	9.17	26.6	20.0	14.4	29.2	24.8	19.9	28.9	25.9	22.8	35.6	32.4	30.2	37.2	38.0	33.6
32								25.8	19.9	24.4	25.4	28.0	33.4	34.3	37.8	42.8	42.2	47.0	48.2	50.8	56.4	55.5	61.1	59.5
33									54.5	19.4	31.4	48.4	33.4	45.2	60.3	51.4	60.6	69.7	65.2	73.1	83.6	80.2	85.3	91.9
41										50.6	35.0	29.6	51.1	47.1	42.9	57.0	53.0	48.7	67.6	63.9	67.1	74.6	78.2	68.4
42											54.6	47.2	54.1	62.8	67.0	78.1	79.8	82.1	94.4	96.8	102	114	116	116
43												92.9	55.1	79.1	106	84.6	105	124	113	128	150	141	154	165
51													96.0	82.0	80.4	106	106	108	134	133	137	156	155	155
52														109	116	129	139	148	158	172	184	202	219	218
53															176	130	168	210	191	209	258	244	268	320
61																176	178	182	230	228	244	275	279	286
62																	221	236	262	279	328	334	369	406
63																		328	292	344	419	378	440	506
71																			355	390	416	485	503	525
72																				439	492	542	578	630
73																					659	598	666	754
81																						722	754	812
82																							825	930
83																								1150

[redacted]

TABLE VI.- CALCULATED NATURAL FREQUENCIES AND MODE SHAPES

Mode	Frequency
f_2	113.2
f_4	347.0
f_6	535.4
f_8	679.8

Normalized mode shape				
Deflection point	Deflection for mode -			
	f_2	f_4	f_6	f_8
11	0.0003	-0.0361	-1.1499	0.2904
12	.0140	-.0544	-.3695	.2586
13	.0200	-.0719	1.1075	1.4555
21	.0203	-.1109	-1.8228	.4693
22	.0454	-.1493	-.4416	.3803
23	.0648	-.1692	2.0711	1.7224
31	.0608	-.2199	-2.3645	.4561
32	.0942	-.2500	-.6276	.4848
33	.1321	-.2897	2.4391	1.0976
41	.1197	-.3538	-2.7251	.5382
42	.1729	-.3498	-.6481	-.0718
43	.2267	-.3612	2.9050	-.2605
51	.2298	-.4249	-2.2276	-.2667
52	.2999	-.3878	.0232	-.5754
53	.3674	-.3254	3.4990	-.8526
61	.3837	-.3889	-1.4172	-.8693
62	.4696	-.1870	.6971	-.9972
63	.5525	-.0048	3.0843	-.7251
71	.6085	.0580	-1.8103	-.3374
72	.6804	.2469	-.6047	.3231
73	.7806	.4025	1.8765	.0562
81	.8374	.5698	-2.6555	.9789
82	.9081	.6881	-1.2504	.8028
83	1.0000	1.0000	1.0000	1.0000

TABLE VII.- EXPERIMENTAL RESULTS FOR MODELS WITH MOUNT FIXED

Wing behavior code: O - Burst of sinusoidal oscillations
D - Start of low damping
F - Flutter
X - Model failure
Q - Maximum q, no flutter

Wing	Run	Code	M	q, lb/sq in.	V, ft/sec	ρ, slugs/cu ft	T, °Rankine	f, cps
Wing with nacelles								
2	17	O	0.899	6.11	945.1	0.0020	460.0	110
		X	1.327	19.46	1,270.2	.0037	381.3	---
*1	18	D	.819	8.26	866.1	.0032	465.4	113
		F	.829	8.66	874.9	.0032	463.6	113
		X	.853	9.29	895.3	.0033	458.5	114
4	19	O	.798	6.50	844.0	.0026	465.5	114
		D	.836	7.28	878.9	.0026	460.0	113
		F	.887	8.28	922.7	.0028	450.4	116
		X	.912	8.90	945.6	.0029	447.4	108
8	20	O	.671	7.97	719.0	.0044	477.9	118
		F	.670	9.00	711.7	.0051	469.6	116
*8	23	O	.801	5.94	842.9	.0024	460.9	---
		F	.855	6.68	891.3	.0024	452.3	111
		X	.885	7.10	917.6	.0025	447.4	104
Wing without nacelles								
7	21	O	0.627	5.16	676.0	0.0032	483.8	190
		O	.638	5.43	686.6	.0033	482.0	192
		F	.631	5.40	679.4	.0034	482.5	183
		X	.621	5.27	669.1	.0034	483.1	---
Semispan models (9- by 18-inch supersonic flutter tunnel)†								
Wings with nacelles		F	1.3	19.23	1,287	0.0033	546	129
		F	1.3	23.60	1,303	.0040	561	136
		Q	1.3	23.82	1,298	.0041	557	---
Wing without nacelles		F	1.3	10.55	1,290	.0018	554	213

*Wing damaged in previous run; repaired prior to present run.
†Four different models used to obtain data.

TABLE VIII.- EXPERIMENTAL RESULTS FOR MODELS WITH MOUNT FREE

IN ROLL AND VERTICAL TRANSLATION

Wing behavior code:
- H - Start of high-frequency oscillations
- O - Burst of regular sinusoidal oscillations
- F - Flutter
- E - End of flutter (dynamic pressure increasing)
- X - Model failure
- Q - Maximum q, no flutter

Wing	Run	Code	M	q, lb/sq in.	V, ft/sec	ρ, slugs/cu ft	T, °Rankine	f, cps
Wing with nacelles								
3	9	H	0.714	4.36	770.0	0.0021	484.0	---
		O	.873	5.94	921.8	.0020	464.0	111
		O	1.150	8.73	1,164.3	.0018	426.6	110
		O	1.289	14.52	1,254.6	.0026	394.3	117
		O	1.311	19.54	1,256.6	.0036	382.4	125
		Q	1.300	23.88	1,232.0	.0045	373.8	---
	10	H	.768	4.93	823.7	.0021	478.7	---
		O	1.141	8.59	1,159.2	.0018	429.6	111
		X	1.304	22.83	1,237.8	.0043	375.0	---
1	12	H	.645	6.28	695.3	.0037	483.6	---
		O	.664	8.74	1,244.8	.0030	388.1	114
Wing without nacelles								
6	11	F	0.790	5.10	839.9	0.0021	470.5	186
		E	.957	6.59	993.6	.0019	448.6	203
		X	1.277	11.28	1,247.1	.0021	396.9	---
5	13	O	.662	7.08	709.5	.0040	478.1	215
		H	.666	7.40	712.8	.0042	476.7	---
		F	.666	7.76	711.5	.0044	475.0	222
		X	.656	7.73	700.7	.0045	474.8	---

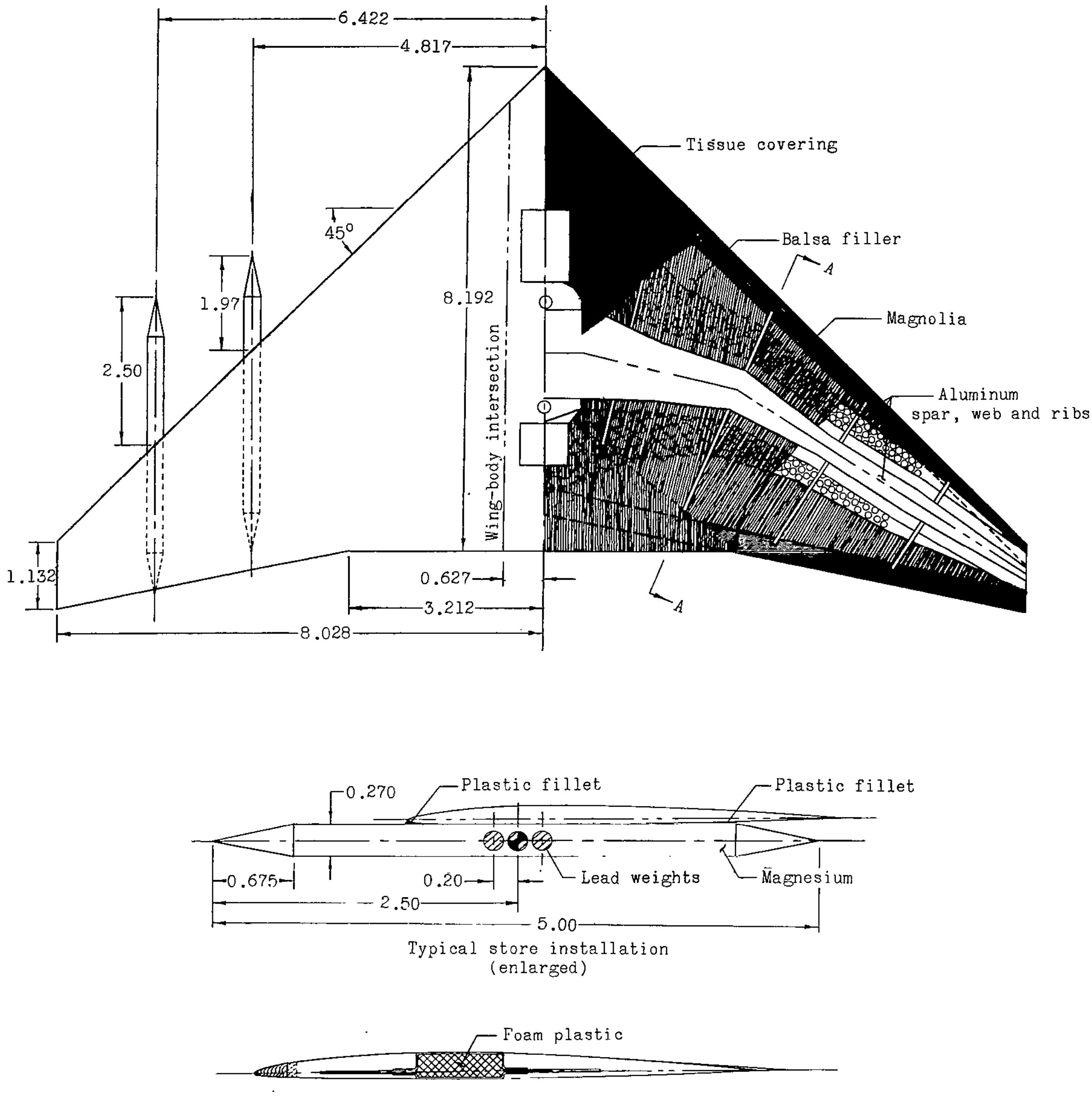

Figure 1.- Configuration and construction details of the wing and stores. (Linear dimensions in inches.)

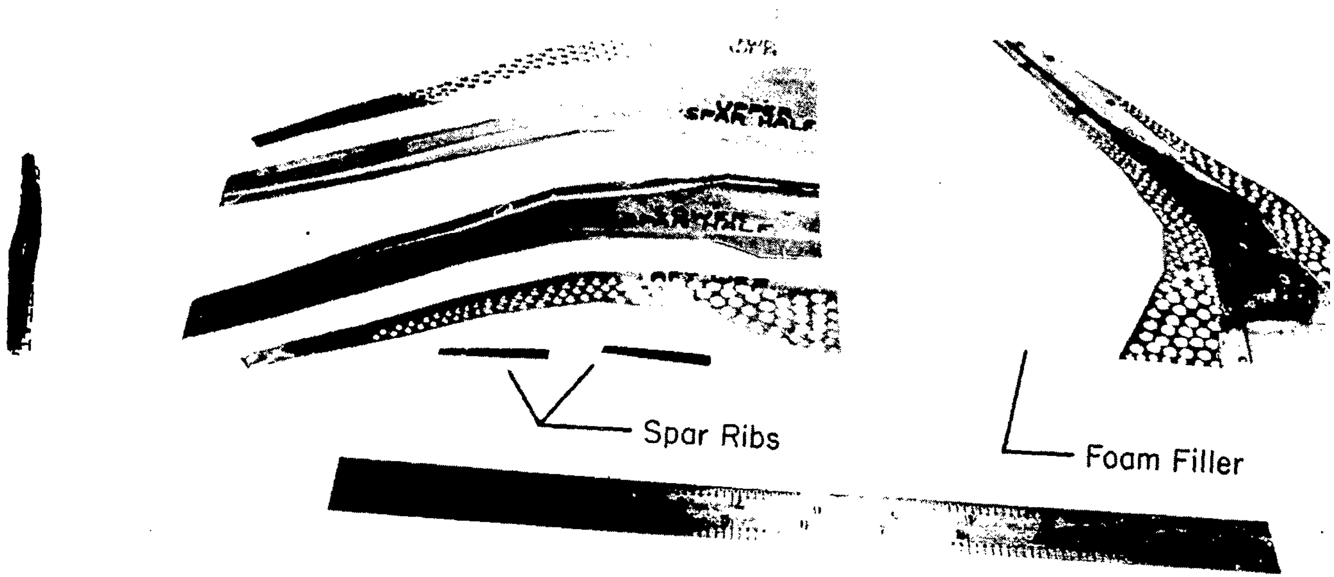

Figure 2.- Photograph of the spar-web assembly. L-9518

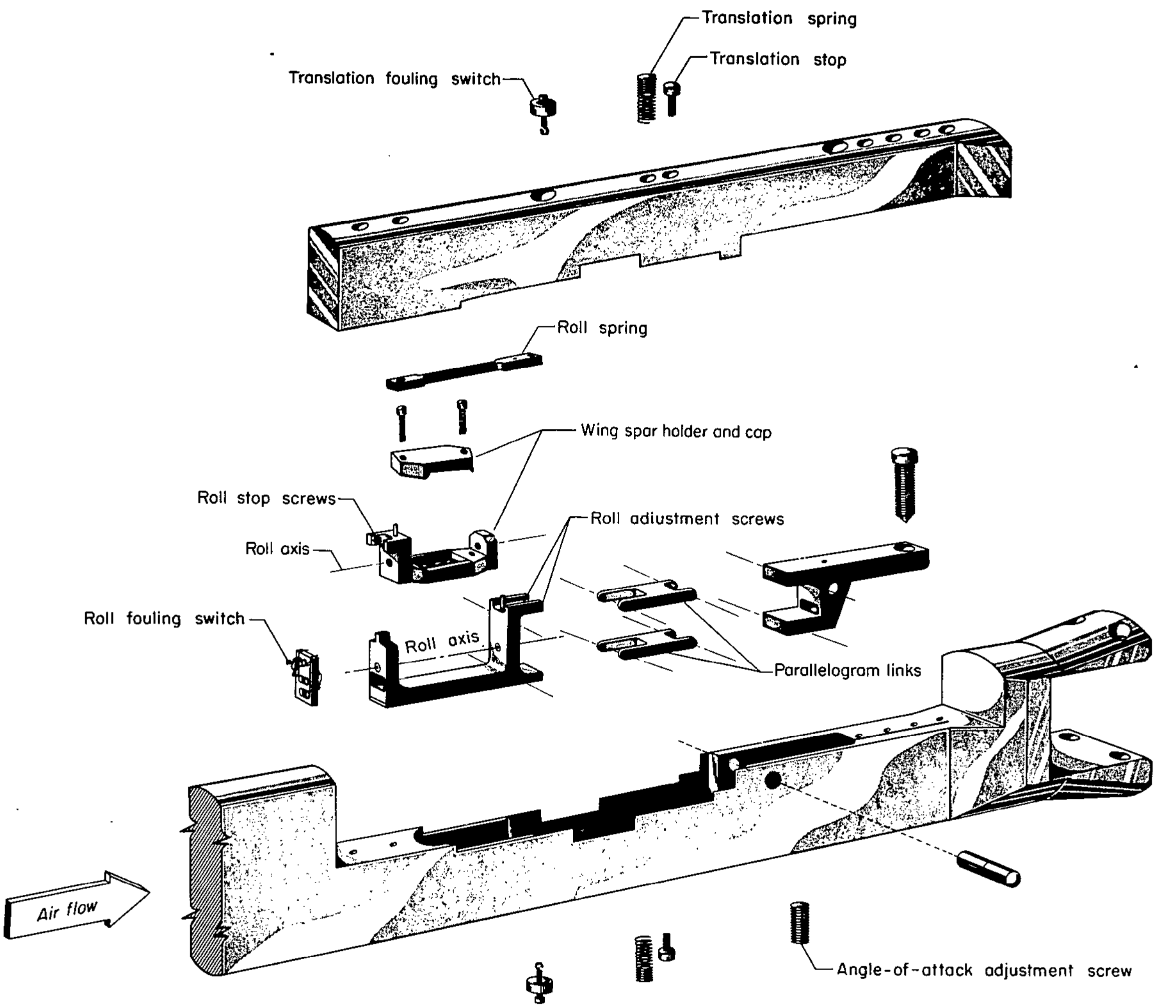

Figure 3.- Exploded view of the sting and wing-mount assembly.

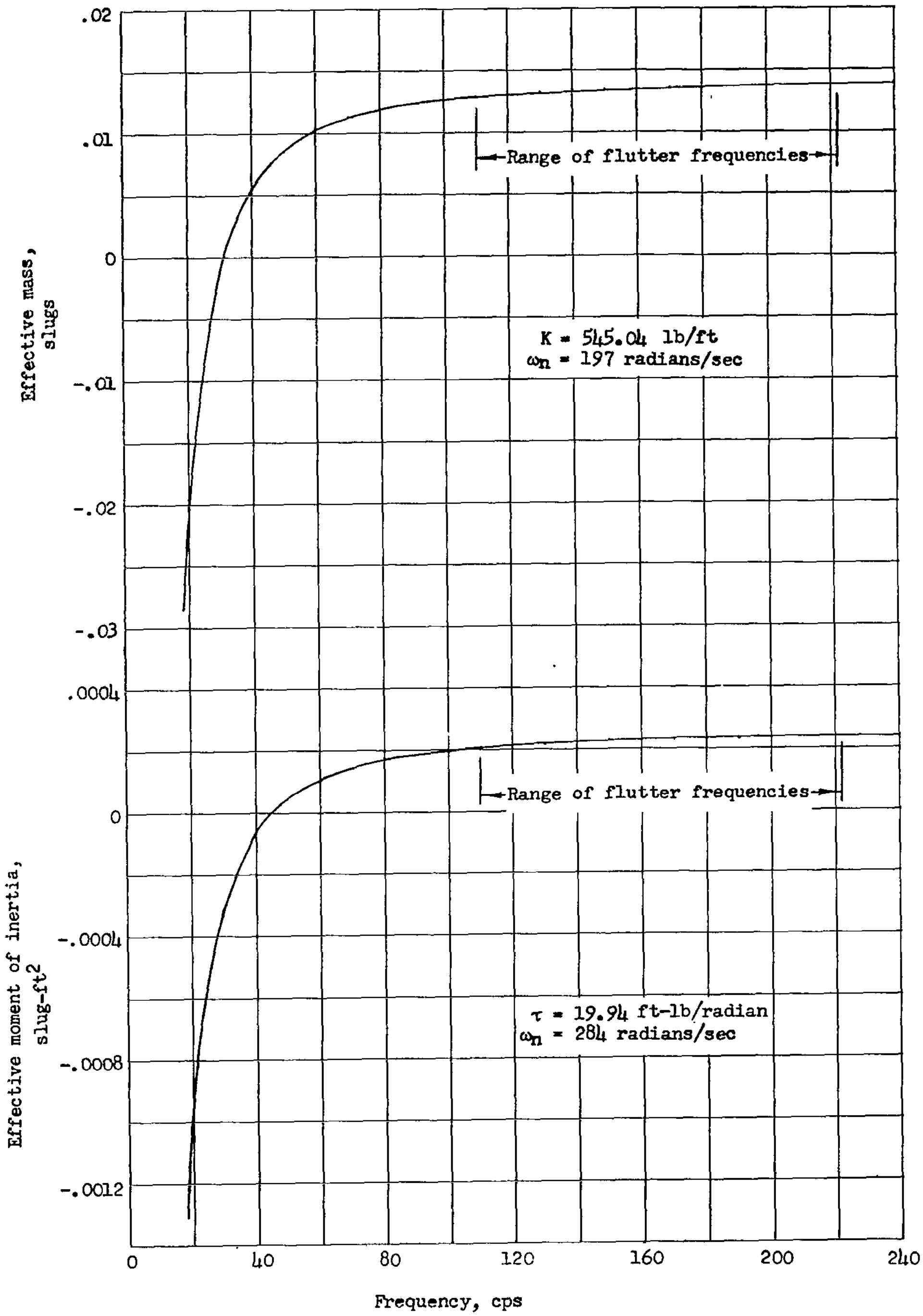

Figure 4.- Effective mass and inertial properties of the wing mounting system.

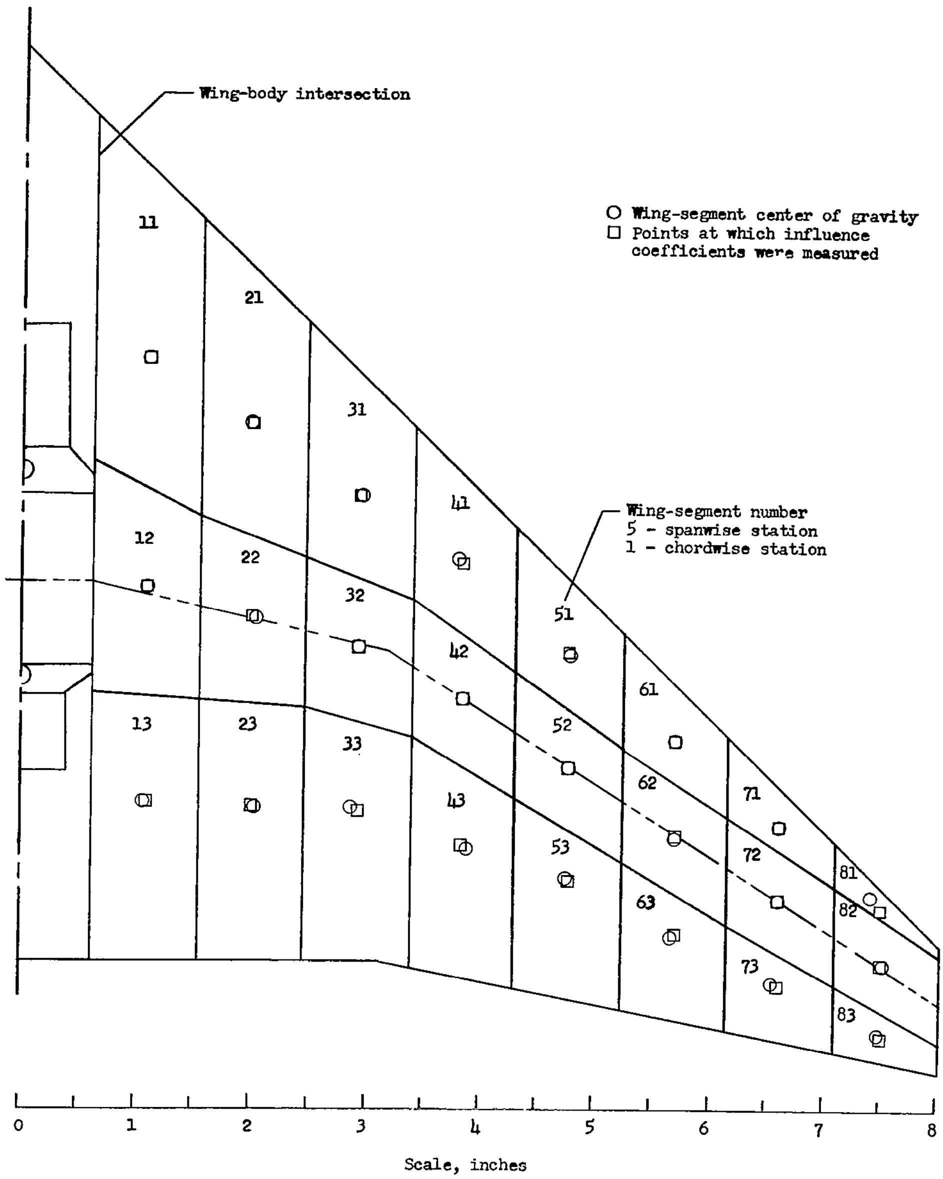

Mass of Wing Segments (slugs × 10^6)

Chordwise station	Spanwise station							
	1	2	3	4	5	6	7	8
1	209.9	189.7	115.6	99.9	64.3	48.1	31.4	10.0
2	207.1	154.6	142.8	131.1	136.7	105.0	101.8	64.9
3	172.2	112.3	106.0	73.7	59.6	39.0	19.5	6.4

Figure 5.- Points at which influence coefficients were measured; location and mass properties of associated wing segments.

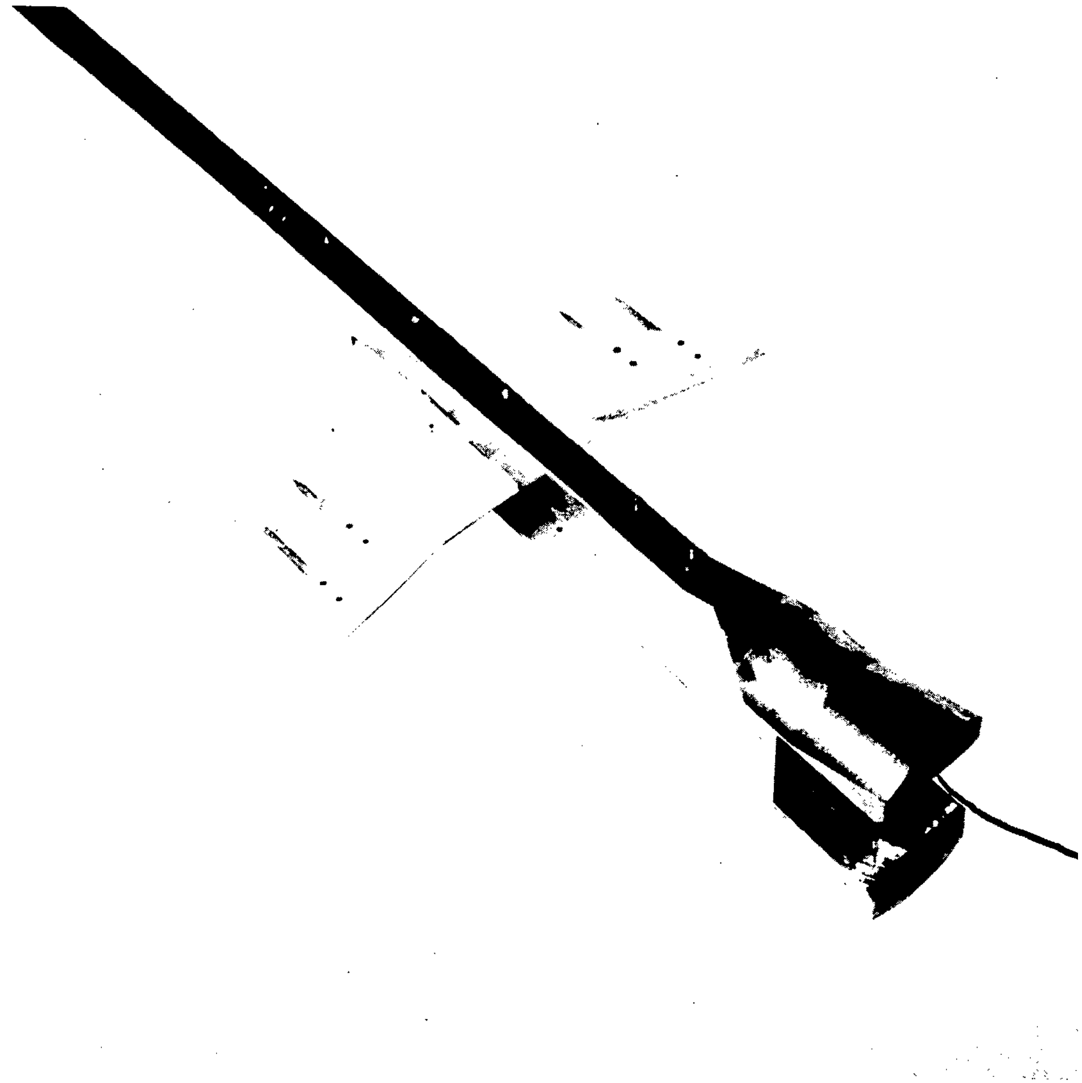

Figure 6.- Model mounted in supporting sting. L-951

[redacted]

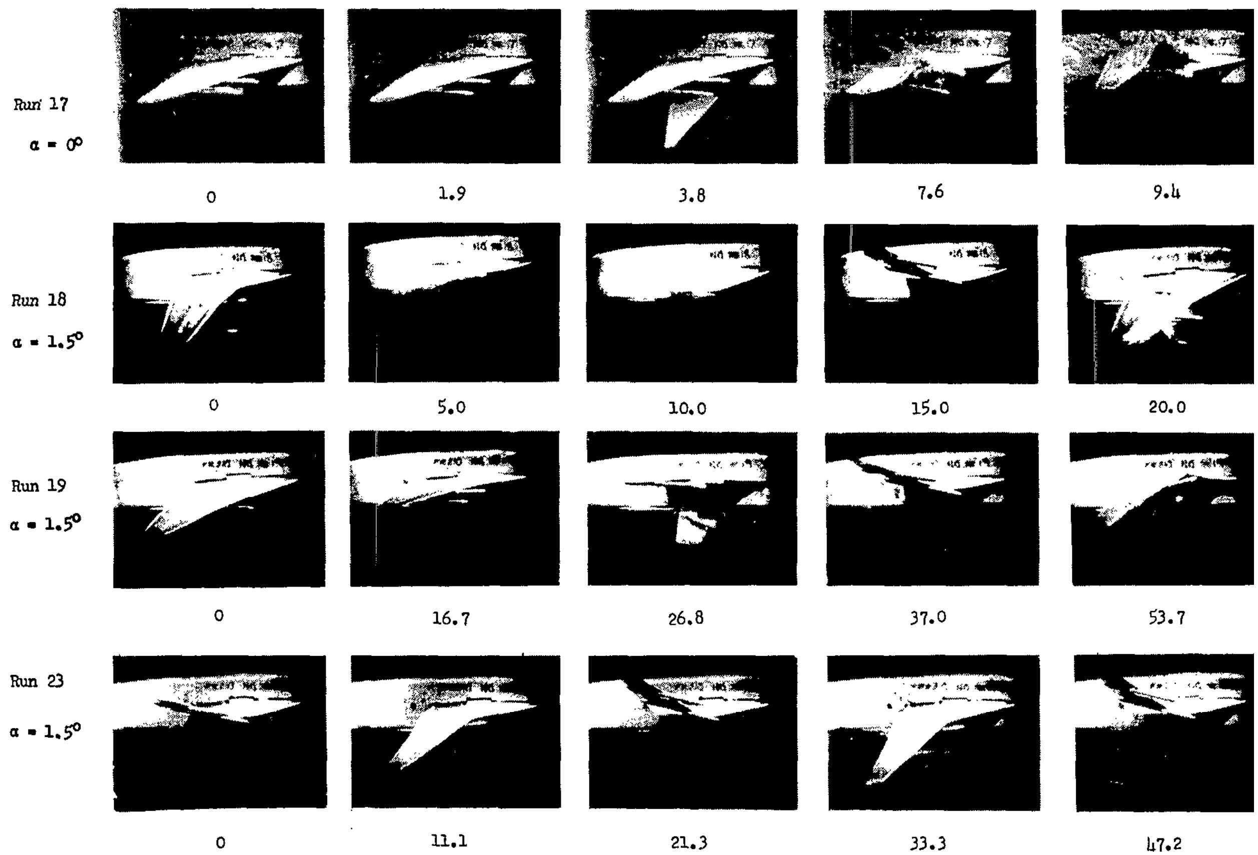

Figure 7.- Selected frames from high-speed motion pictures of model failur
frames indicate time elapsed in thousandths of a second.

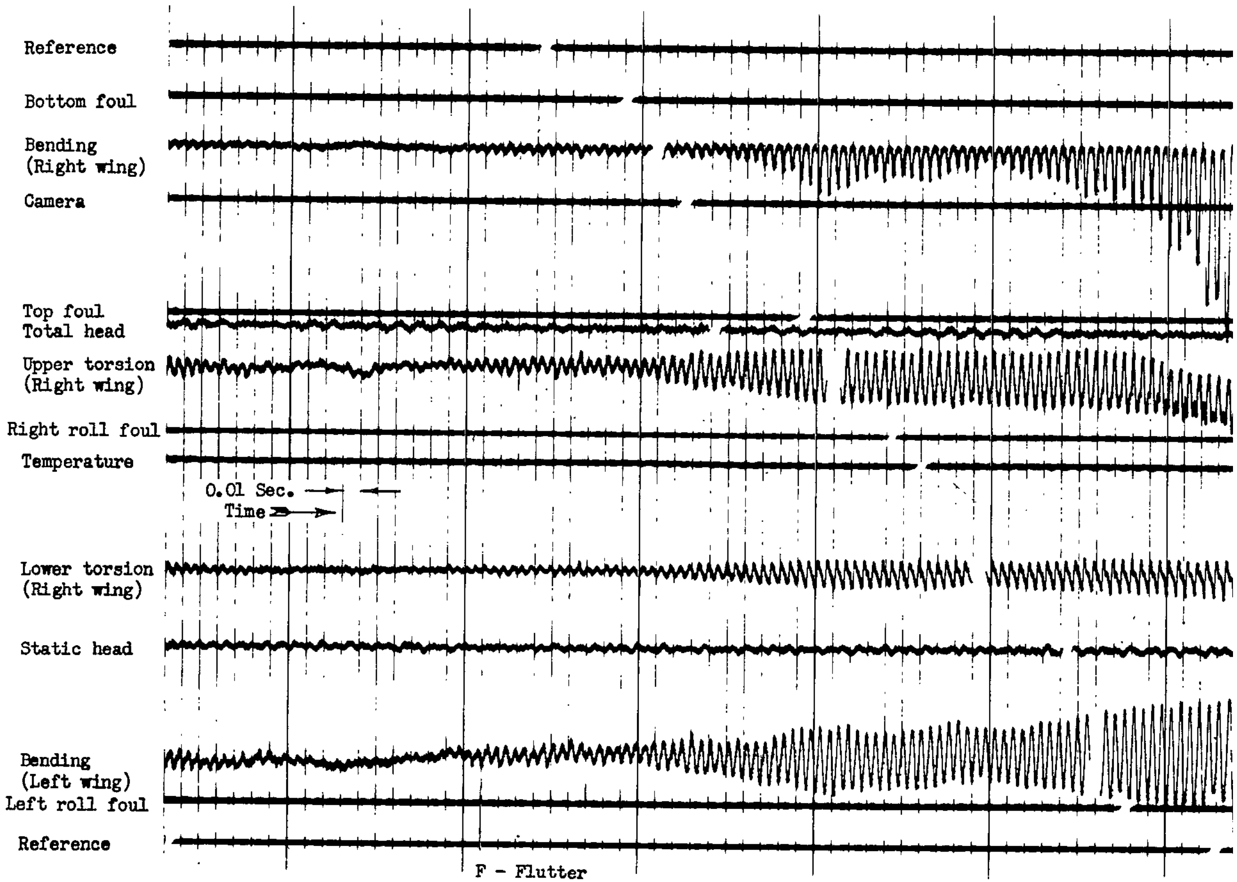

Figure 8.- Sample oscillograph record of test with wing mount fixe

[redacted]

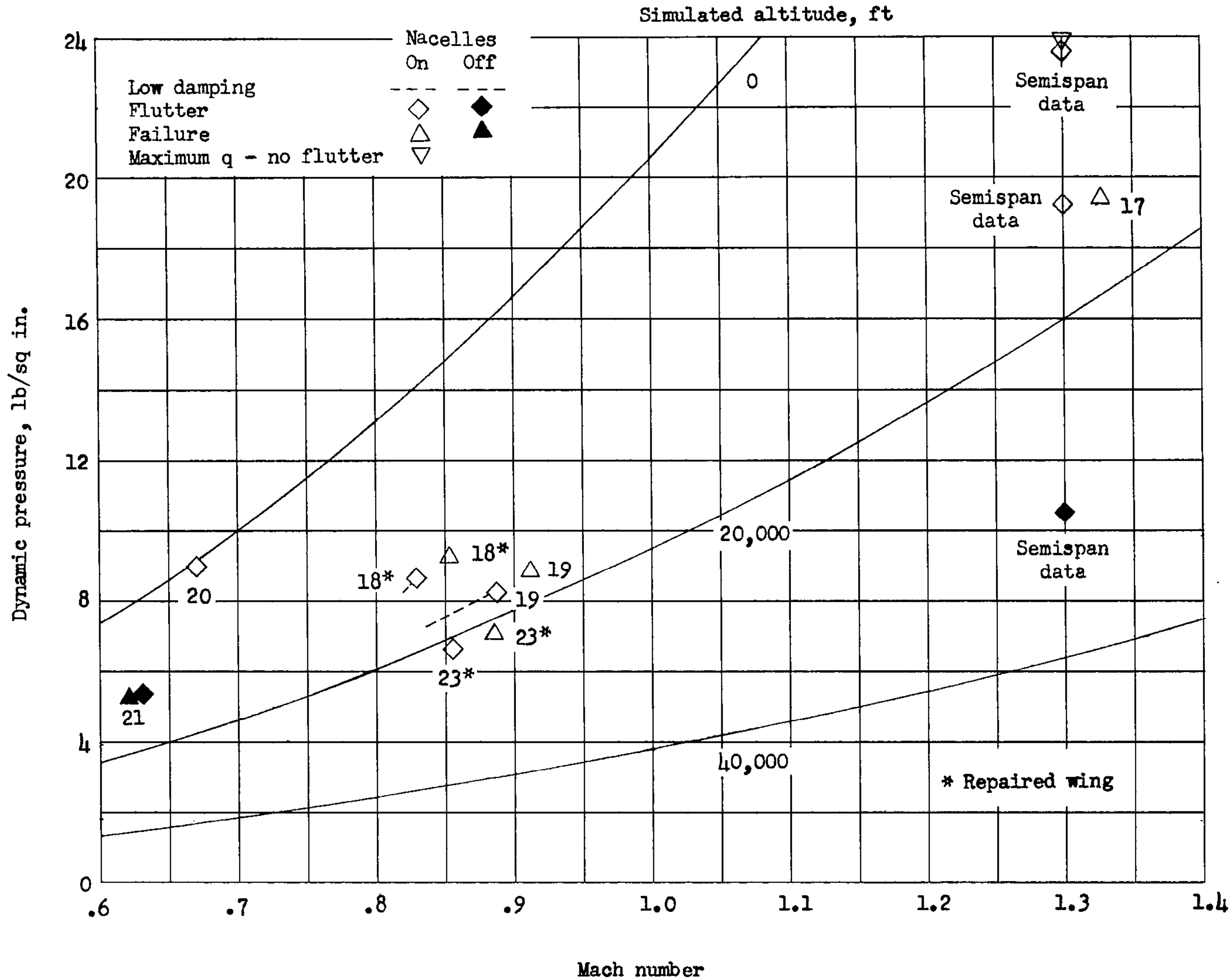

Figure 9.- Experimentally determined flutter characteristics of the wing with mount fixed. (Numbers denote run.)

[redacted]

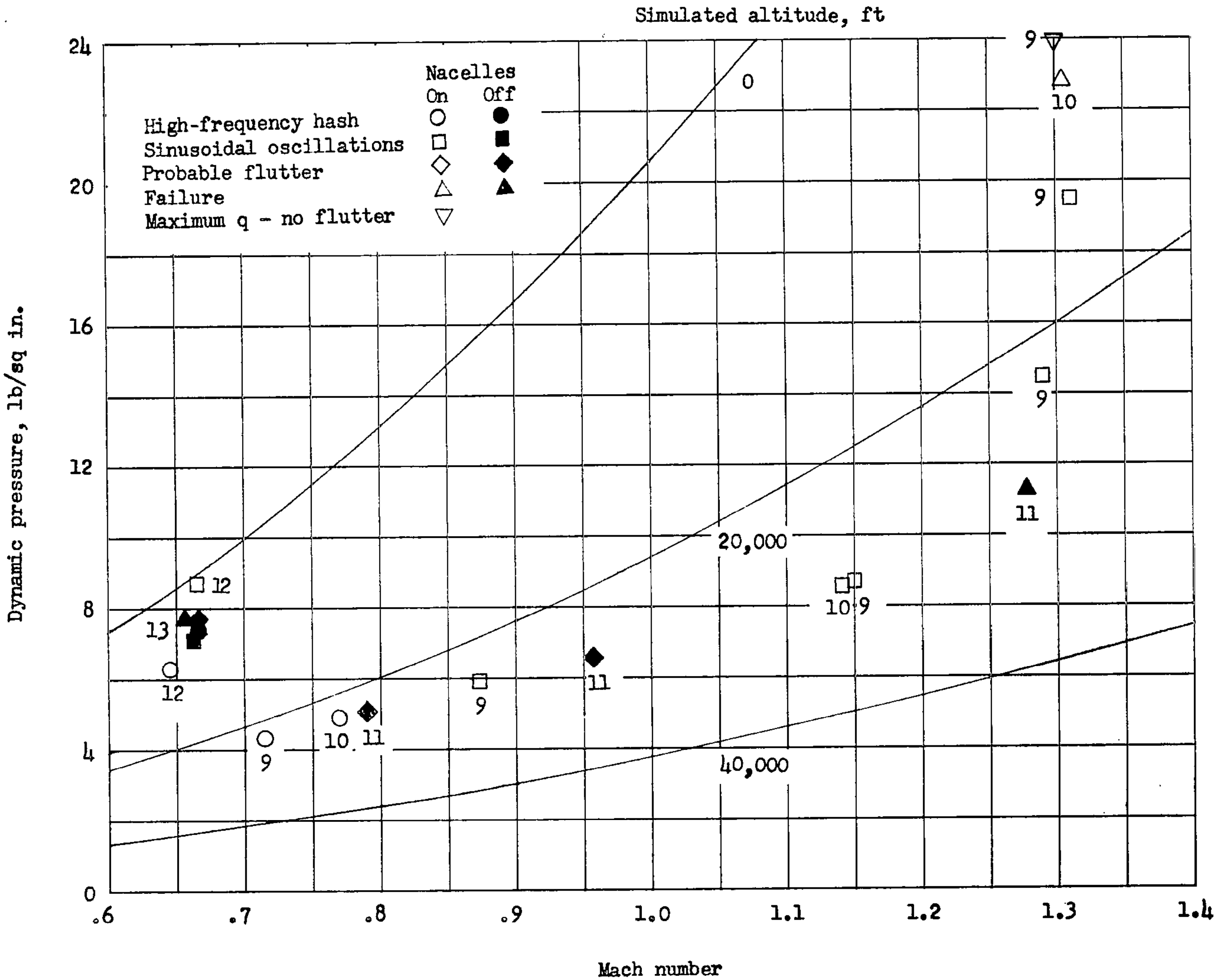

Figure 10.- Experimentally determined flutter characteristics of the wing mount with freedom in roll and vertical translation. (Numbers denote run.)

CONFIDENTIAL